



FULL PAPER

Electrocatalytic properties of a dinuclear cobalt(III) coordination compound in molecular oxygen reduction reaction

Mohammad Ali Kamyabi¹ | Fatemeh Soleymani-Bonoti¹ | Fariba Alirezaei¹ |
Rahman Bikas² | Nader Noshiranzadeh¹ | Marzieh Emami¹ |
Marta S. Krawczyk³ | Tadeusz Lis⁴

¹Department of Chemistry, Faculty of Science, University of Zanjan, 45371-38791 Zanjan, Iran

²Department of Chemistry, Faculty of Science, Imam Khomeini International University, 34148-96818 Qazvin, Iran

³Department of Analytical Chemistry, Faculty of Pharmacy, Wrocław Medical University, Borowska 211A, 50-556 Wrocław, Poland

⁴Faculty of Chemistry, University of Wrocław, Joliot-Curie 14, 50-383 Wrocław, Poland

Correspondence

Mohammad Ali Kamyabi, Department of Chemistry, Faculty of Science, University of Zanjan 45371-38791. Zanjan, Iran.
Email: makamyabi@gmail.com

A new dinuclear cobalt(III) coordination compound, $[\text{Co}_2\text{L}(\mu\text{-N}_3)(\text{N}_3)_2]\cdot\text{CH}_3\text{OH}$ (**1**), was synthesized and characterized by elemental analysis, spectroscopic methods, and single-crystal X-ray analysis in which H_3L is a heptadentate ligand obtained by the condensation of triethylenetetramine with 5-bromo-2-hydroxybenzaldehyde. X-ray analysis revealed that two cobalt(III) ions have distorted octahedral geometry and are connected together by a phenoxy and an azide bridging ligand. The catalytic activity of compound **1** for oxygen (O_2) reduction reaction was investigated. Compound **1** can efficiently catalyze the reduction of O_2 by a weak electron donor, ferrocene (Fc), at the polarized water–1,2-dichloroethane interface. It was found that compound **1** can catalyze O_2 reduction to H_2O_2 , whereas in the presence of Fc, it can catalyze the reduction of O_2 to water.

KEYWORDS

dinuclear cobalt(III) coordination compound, ferrocene, liquid–liquid interface, oxygen reduction reaction

1 | INTRODUCTION

The respiratory oxygen (O_2) reduction reaction (ORR) can be carried out with energy metabolism in aerobic organisms for building up a transmembrane proton gradient to power the adenosine triphosphate synthesis.^[1] The ORR proceeds either by a $4\text{e}^-/4\text{H}^+$ pathway, which can produce water, or by a $2\text{e}^-/2\text{H}^+$ way to yield H_2O_2 , which is considered a green oxidant.^[2] ORR is a spin-forbidden process, so it is kinetically slow at ambient temperature unless a catalyst is present.^[3–6] Heterogeneous electrocatalytic study of ORR by modification of an electrode surface with a catalyst often induces changes in the catalyst morphology. For solving this problem, a homogeneous pathway using a molecular electron donor compound, such as

ferrocene (Fc), was proposed by Fukuzumi et al.^[7,8] In homogeneous ORRs, mononuclear metal complexes catalyze O_2 reduction to H_2O_2 , whereas bimetallic complexes catalyze the reduction to H_2O . By performing a comparison between the solid–solution interface and liquid–liquid interface, electrochemical measurements at the liquid–liquid interface allow the monitoring of both ion and electron transfers while in solid–solution interface only electron transfer can occur.^[9]

Polarizable soft interfaces between two immiscible electrolyte solutions (ITIES) have emerged as model charge transfer reactions (electron and ion transfer) that impact energy research, mainly the hydrogen evolution reaction^[10] and ORR.^[11] These model reactions can also be used in solvent-extraction processes, chemical sensing,

solar-energy-conversion systems, drug release, and drug delivery.^[2,12] The ORR can be driven by the interfacial Galvani potential difference at ITIES. Galvani potential can be controlled potentiostatically or chemically by using a four-electrode potentiostat or the distribution of electrolyte ions dissolved in both phases. ORR at the liquid–liquid interfaces has been studied using various lipophilic electron donors, such as Fc,^[12–14] tetrathiafulvalene,^[15] decamethylferrocene (DMFc),^[16] and tetrachloroquinone.^[17]

The cobalt coordination compounds have been widely used as catalysts in reactions such as oxidation of alkanes and alkylbenzenes,^[18,19] water oxidation,^[20] CO₂ reduction,^[21] converting CO and carboxylic acids^[22] to methanol,^[23] hydrogenation of nitriles to primary amines,^[24] converting proton ions to hydrogen molecules,^[25] and hydrogen evolution.^[26] These compounds have also been used as catalysts for ORR at the liquid–liquid interface.^[5,27–29] Whereas the single-core cobalt complexes produced more hydrogen peroxide, dinuclear and multinuclear cobalt complexes catalyzed a four-electron pathway reduction of O₂ to water.^[30–33]

In this work, the catalytic role of a new dinuclear Co(III) coordination compound (**1**) in ORR was investigated by ion-transfer voltammetry and biphasic shake-flask experiments based on UV–visible spectroscopy measurements. The results showed that compound **1** can catalyze the reduction of O₂ to H₂O. In addition, the results confirmed that the catalytic effect of compound **1** arises from the activation of O₂ by two cobalt ions in the structure of this compound.

2 | EXPERIMENTAL

2.1 | Materials and instrumentations

See the Supporting Information File.

2.2 | Synthesis of the compound [Co₂(L)(μ-N₃)(N₃)₂]·CH₃OH (**1**)

The reaction of H₃L and cobalt(II) chloride hexahydrate in methanol led to the formation of a new Co(III) coordination compound. This compound was synthesized by the reaction of H₃L (0.695 g, 1 mmol), CoCl₂·6H₂O (0.475 g, 2 mmol), and sodium azide (2.6 g, 4 mmol) in a branched tube using methanol as solvent. The aforementioned amounts of these materials were placed in the main arm of the branched tube. Methanol was carefully added to fill the arms and the tube was sealed. The reagents-containing arm was then immersed in an oil bath at 60 °C while the other arm was maintained at

ambient temperature. After 3 days, dark violet-red crystals appeared in the cooler arm, which were separated and washed by cold methanol. *Caution! Although we have not experienced any problem with the reported compound in this work, azide complexes of metal ions are potentially explosive and should be handled with care.* Yield 85%. Anal. Calc. for C₂₈H₂₈Br₃Co₂N₁₃O₄ [molecular weight = 968.22 g mol⁻¹]: C, 34.74; H, 2.91; N, 18.81; Co, 12.17. Found: C, 34.78; H, 2.96; N, 18.94; Co, 12.14%. Fourier transform-infrared (FT-IR) (KBr, cm⁻¹): 3431 (m, br), 2924 (w), 2853 (w), 2095 (vs), 2023 (vs), 1629 (s), 1591 (m), 1519 (w), 1434 (s), 1453 (s), 1426 (w), 1379 (w), 1316 (m), 1291 (w), 1275 (w), 1258 (m), 1239 (w), 1201 (w), 1175 (w), 1137 (w), 1093 (w), 1066 (w), 1029 (m), 950 (m), 878 (w), 873 (w), 820 (m), 802 (w), 690 (m), 660 (w), 640 (w), 600 (w), 547 (w), 535 (w), 462 (m), 450 (m). UV–Vis in CH₃OH, c = 2.5 × 10⁻⁵ M, λ_{max} 283 nm with ε = 1.6 × 10⁻⁷ M⁻¹ cm⁻¹.

2.3 | X-ray crystallography

Data collection for X-ray structure determination was performed on an Oxford XCALIBUR PX automated four-circle diffractometer with a CCD Ruby detector using graphite monochromatized Mo-K_α radiation (λ = 0.71073 Å) at 90 K (Oxford Cryosystems cooler). The crystal data and refinement parameters are presented in Table 1 and other details are available in the supporting information file.

2.4 | Electrochemical measurements

A commercial micropotentiostat (PGSTAT101, Eco Chemie) was used for voltammetry measurements at the water–1,2-dichloroethane (DCE) interface in a four-electrode cell. This cell was organized as a three-compartment glass cell. Two platinum counter electrodes and two reference electrodes, silver/silver chloride (Ag/AgCl), were positioned in the aqueous and DCE phases, respectively. Luggin capillary was used for applying the external potential. The reversible half-wave potential of the TMA⁺ cation transfer (0.16 V) was employed for converting the potential of the system to the Galvani potential difference (Δ_o^{wφ}).^[34] All electrochemical measurements were performed at ambient temperature (25 ± 1 °C).

2.5 | The Galvanic cell experiments

Galvanic experiments were performed in a small flask under constant stirring conditions. The flask was filled with DCE solution (1 mL) containing 4 mM Fc and 1 mL

TABLE 1 Crystallographic data of compound **1**

Compound	[Co ₂ (L)(μ-N ₃)(N ₃) ₂].CH ₃ OH (1)
Formula	C ₂₇ H ₂₄ Br ₃ Co ₂ N ₁₃ O ₃ .CH ₄ O
M _r (g mol ⁻¹)	968.22
Crystal size (mm)	0.40 × 0.14 × 0.12
Crystal shape, color	Needle, dark violet-red
Temperature (K)	90
Radiation (Å)	Mo-K _α (λ = 0.71073)
Crystal system	Monoclinic, P ₂ ₁ /n (No. 17)
a (Å)	9.9350(19)
b (Å)	23.755(5)
c (Å)	13.963(3)
β (degrees)	92.96(2)
V (Å ³)	3291.0(12)
Z	4
Calculated density (mg m ⁻³)	1.954
μ (mm ⁻¹)	4.71
Measured reflections	23,806
Independent reflections	9646
R _{int}	0.031
h, k, l	-11 → 14, -30 → 33, -19 → 17
θ range	2.9–31.2
Parameters	453
F(000)	1912
R[F ² > 2σ(F ²)]	0.033
wR(F ²)	0.063
S	1.03
R _{int}	0.031
Δρ _{Max} /ρ _{Min} (e Å ⁻³)	0.54/−0.46

of aqueous solution containing 50 μM of compound **1** and 10 mM of HCl, respectively. The salt lithium tetrakis(pentafluorophenyl)borate ethyl etherate (LiTB, for the common ion TB⁻) was added at a concentration of 5 mM to the aqueous phase. After stirring the two-phase mixture for 30 min, the two phases were separated from each other. These two separated solutions were then treated by excess amount of potassium iodide (KI) and used for UV–Vis spectroscopy measurements.

3 | RESULTS AND DISCUSSION

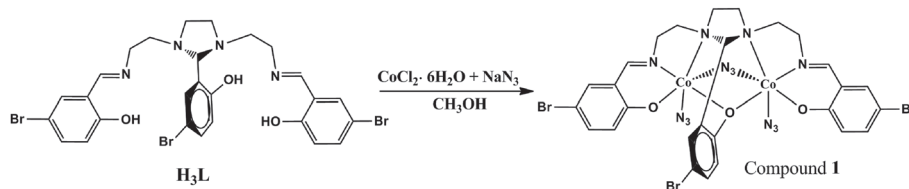
3.1 | Synthesis and spectroscopy

The reaction of triethylenetetramine with 5-bromosalicylaldehyde at a molar ratio of 1:3 in methanol produced

the desired symmetric heptadentate Schiff base ligand H₃L (Scheme 1). Elemental analyses and spectroscopic data confirmed the synthesis of the ligand.^[35] Compound **1** was synthesized by the reaction of H₃L, NaN₃, and CoCl₂·6H₂O at a molar ratio of 1:4:2 in methanol. The infrared spectrum of compound **1** showed a band at 1623 cm⁻¹ which was assigned to the C=N stretching frequency of the coordinated Schiff base ligand. Furthermore, in the FT-IR spectrum of compound **1** two very strong bands were observed at 2095 and 2023 cm⁻¹, which were assigned to the terminal and bridged azide stretching vibrations, respectively.^[36] These bands were considered as new peaks for **1** since they were not observed in the FT-IR spectrum of the free ligand. A very broad band at 3430 cm⁻¹ confirmed the presence of –OH group of the uncoordinated methanol molecule involved in hydrogen bonding interactions.

3.2 | X-ray structure of compound **1**

The molecular structure of compound **1** is shown in Figure 1 and selected bond distances and angles are summarized in Table 2. Single-crystal X-ray analysis indicated that compound **1** is a neutral dinuclear coordination compound of cobalt(III), with a methanol molecule existing as molecule of solvent in the crystal. In this structure, two cobalt atoms are doubly bridged by a phenolate atom (O2C) from the central phenolate arm of the Schiff base ligand and a nitrogen atom (N1) provided by the azide bridging group. The Schiff base ligand acts as a heptadentate trianionic compartmental donor, with two tridentate N₂O cavities and a central bridging phenolate group. Both cobalt centers are six-coordinated with *cis*-[CoN₄O₂] coordination environment and the coordination geometry around them can be described as distorted octahedral geometry. One oxygen atom and two nitrogen atoms of the Schiff base ligand occupy three coordination sites of each cobalt core and the remaining three sites are occupied by the oxygen atom of the phenoxy bridging group and two nitrogen atoms of two (one terminal and one bridging) azide ligands. Two Co(III) ions form nearly planar four-membered Co₂NO cyclic units in which the Co...Co distance is 2.9091(7) Å. The intraring Co1–N1–Co2 and Co1–O2C–Co2 angles are 96.43(8)° and 94.97(6)°, respectively. In compound **1** the bridging and terminal azide ligands show asymmetric N–N distances [N1–N2/N2–N3 = 1.240(3)/1.122(3) Å; N4–N5/N5–N6 = 1.209(3)/1.157(3) Å and N7–N8/N8–N9 = 1.208(3)/1.158(3) Å] and the N–N–N angles in all of them is near to linear (≈176°), representing the typical shape of azide ligands.^[37,38] The Co–N and Co–O bond lengths are in the normal range reported for Co(III) coordination



SCHEME 1 Synthesis of compound 1

compounds.^[39–41] The crystal package of compound 1 is stabilized by several O–H···N, C–H···N, C–H···O, C–H···Br, and C–H··· π interactions (Table 3, Figure 2).

3.3 | Cyclic voltammetry of compound 1

Figure 3 illustrates the typical cyclic voltammograms of the ligand and compound 1 which have one and two voltammetric waves, respectively. The Co(II)/Co(I) couple has a redox potential at -0.051 V^[42] (see peak I in Figure 3) and an irreversible peak at 1.01 V which is suggested to be possibly related to the Co(III)/Co(II) couple of compound 1. The small shoulder near this couple can be related to the ligand.

The ion-transfer voltammograms of compound 1 (300 μ M) in the organic phase of the water–DCE interface (cell 1 in Scheme 2) are shown in Figure 4. In the absence of compound 1 at the organic phase, the transfer of Cl^- and H^+/Li^+ from the aqueous phase to the organic phase limits the potential window at positive and negative potentials, respectively. In the presence of compound 1 in the organic phase, one voltammetric wave can be seen. This peak has half-wave Galvani potential of 0.02 V and a peak-to-peak separation of about 57 mV at a scan rate of 50 mV/s. The peaks current depends linearly on

TABLE 2 Selected geometrical parameters (\AA , degrees) for compound 1

Bond	Lengths/ \AA	Bond	Angles/ degrees
Co1–O2A	1.8703(17)	N1–Co1–N4	95.73(8)
Co1–N1A	1.8898(19)	O2A–Co1–O2C	88.66(7)
Co1–N1	1.9432(18)	N1A–Co1–O2C	91.03(7)
Co1–N4	1.944(2)	N1–Co1–O2C	82.48(7)
Co1–O2C	1.9847(16)	N4–Co1–O2C	178.14(7)
Co1–N2A	2.019(2)	O2A–Co1–N2A	179.07(7)
Co1–Co2	2.9091(7)	N1A–Co1–N2A	86.14(8)
Co2–O2B	1.8705(17)	N1–Co1–N2A	89.64(8)
Co2–N1B	1.895(2)	N4–Co1–N2A	89.04(8)
Co2–N7	1.9360(19)	O2C–Co1–N2A	91.48(7)
Co2–N1	1.9582(19)	O2B–Co2–N1B	95.35(8)
Co2–O2C	1.9618(15)	O2B–Co2–N7	92.31(8)
Co2–N2B	2.012(2)	N1B–Co2–N7	89.73(8)
		O2B–Co2–N1	89.49(8)
		O2B–Co2–O2C	86.81(7)
Co1–N1–Co2	96.43(8)	N7–Co2–N1	93.15(8)
Co2–O2C–Co1	94.97(6)	N1B–Co2–N2B	86.01(8)
O2A–Co1–N1A	94.78(8)	N1–Co2–O2C	82.70(7)
O2A–Co1–N1	89.47(8)	N1B–Co2–O2C	94.49(7)
N1A–Co1–N1	172.17(8)	N7–Co2–N2B	88.66(8)
O2A–Co1–N4	90.79(8)	N1–Co2–N2B	89.10(8)
N1A–Co1–N4	90.79(8)	O2C–Co2–N2B	92.12(7)

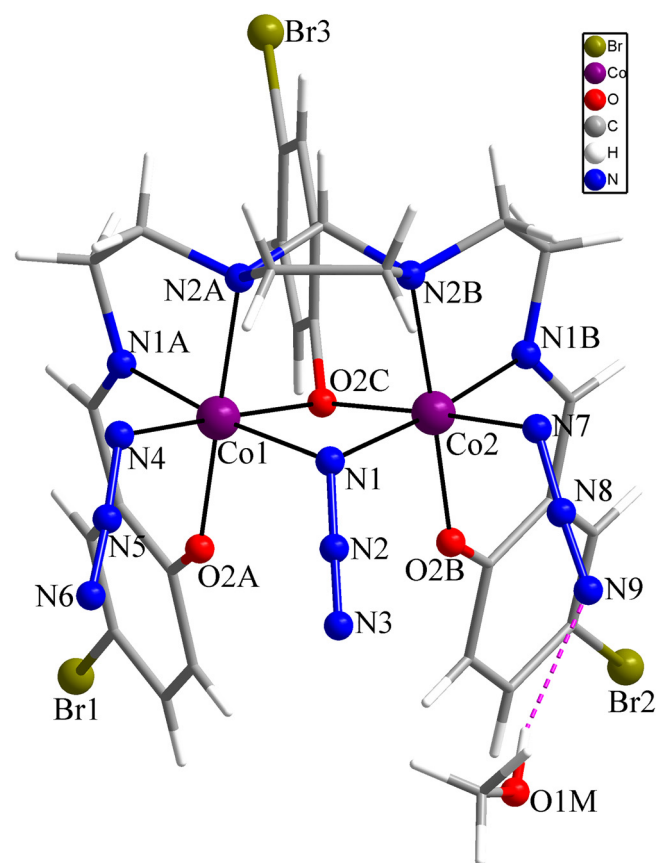


FIGURE 1 Molecular structure of compound 1, $[\text{Co}_2(\text{L})(\mu\text{-N}_3)(\text{N}_3)_2]\cdot\text{CH}_3\text{OH}$

TABLE 3 Hydrogen bonding interactions in the crystal package of compound **1**

D–H...A	D–H/ Å	H...A/ Å	D...A/ Å	D–H...A/ $^{\circ}$
C8A–H8A1...Br1 ⁱ	0.99	2.83	3.652(3)	141
C8B–H8B1...Br1 ⁱⁱ	0.99	2.82	3.585(2)	135
C10A–H10A...N4	0.99	2.57	3.116(3)	115
C9B–H9B2...N3 ⁱⁱⁱ	0.99	2.40	3.186(4)	135
C10B–H10D...N7	0.99	2.54	3.083(3)	115
O1M–H1M...N9	0.84	2.25	3.066(3)	163

Symmetry codes: i = $-x + 2, -y + 1, -z + 1$; ii = $-x + 1, -y + 1, -z + 1$; iii = $x - 1/2, -y + 1/2, z - 1/2$.

the square root of scan rate. Thus, based on these data, it can be concluded that the transfer of compound **1** at the interface is controlled by diffusion (illustrated in Figure 4).

3.4 | The catalytic effect of compound **1** on oxygen reduction reaction

Figure 5 shows the first scan of cyclic voltammograms obtained with cell 2 (Scheme 1) in the presence of 5 mM Fc and various concentrations of compound **1**. In the presence of Fc, a small wave around 0.0 V can be observed which corresponds to the transfer of some traces of ferrocenium (Fc^+) in the system (Figure 5). When both compound **1** and Fc were present, a large irreversible positive current wave was observed at

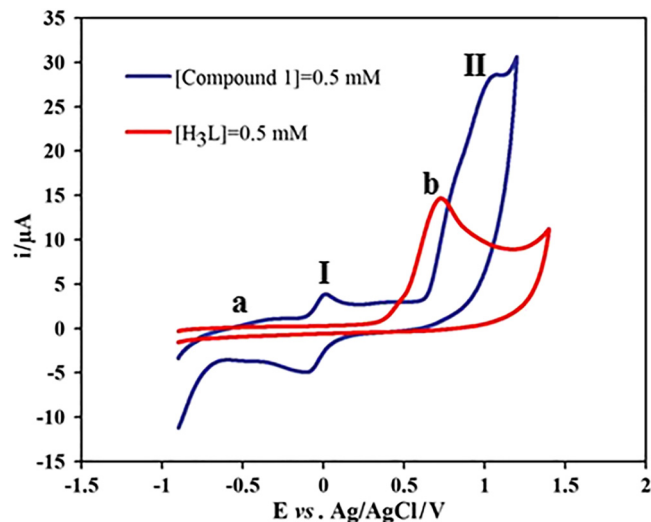


FIGURE 3 Cyclic voltammograms at 0.1 V s^{-1} of (a) compound **1** (0.5 mM) dissolved in 1,2-dichloroethane containing tetrabutylammonium perchlorate (0.1 M) as the supporting electrolyte and (b) H_3L (0.5 mM). In this study a glassy carbon electrode (3 mm), platinum wire, and Ag/AgCl were employed as the working, counter, and reference electrodes, respectively

positive potentials. Irreversible positive current is a wave without a signal on the return scan. The voltammetric signal at positive potentials corresponds to the proton-coupled electron transfer (PCET) reaction. However, on return scan a current wave for the transfer of Fc^+ was observed, indicating that Fc^+ was produced when the interface is positively polarized. In addition, the observed

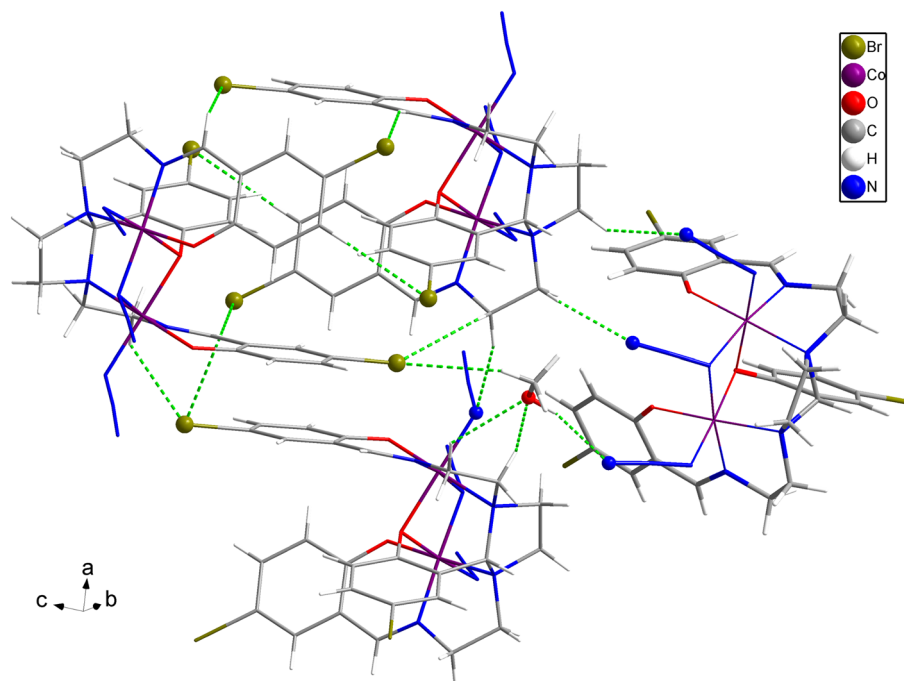
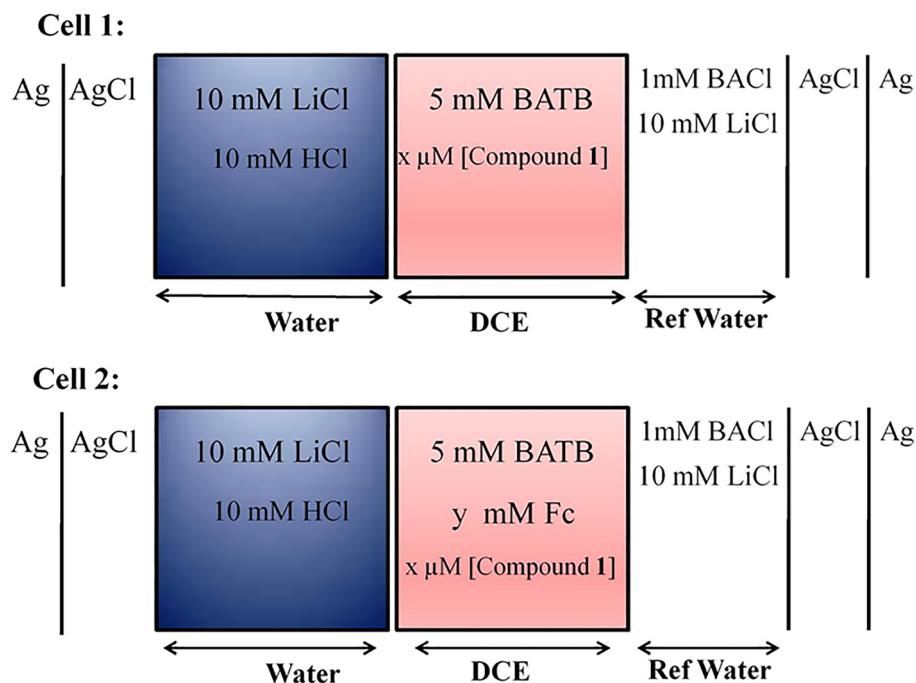


FIGURE 2 Part of intermolecular hydrogen bonding interactions in the crystal packing of compound **1** which are shown as dashed green lines



SCHEME 2 Composition of the electrochemical cells used in this work. DCE, 1,2-dichloroethane; Fc, ferrocene

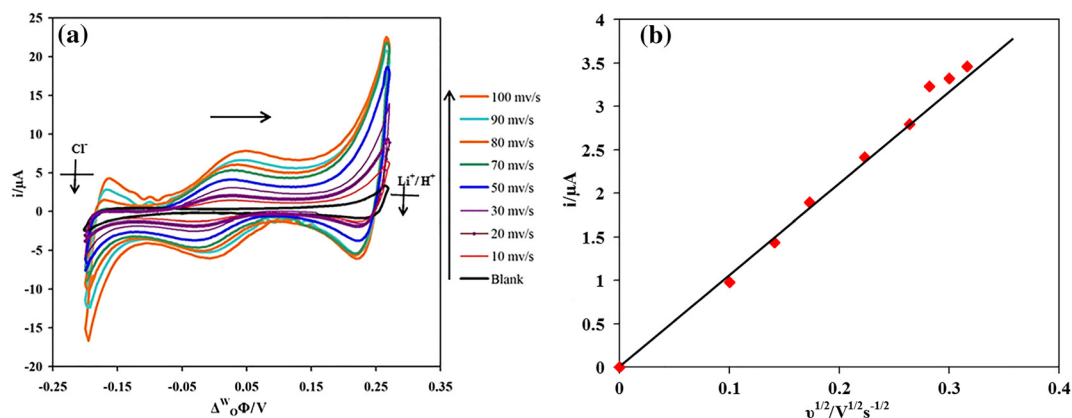


FIGURE 4 (a) Cyclic voltammograms of compound **1** in 1,2-dichloroethane (DCE; Scheme 2, cell 1) at various scan rates (10, 20, 30, 50, 70, 80, 90, and 100 mV/s); (b) linear dependence of the ion-transfer current on the square root of the scan rate [using cell 1 ($y = 50$) of compound **1** in 1,2-DCE]

PCET current and Fc^+ formation also increase with increasing of the concentrations of compound **1** in the range of 0–50 μM (see Figure 5b). The data presented in Figure 5b suggest that the transfer of protons is facilitated by Fc and compound **1**.

3.5 | The Galvanic cell experiments

Two-phase reactions controlled by chemical polarization, so-called shake-flask experiments, were performed. Scheme 3 shows the details of solution composition in the two-phase reactions. In the shake-flask experiments, the common ion (TB^-) is used for

polarization of the interface (obtained by dissolving 5 mM of bis(triphenylphosphoranylidine)ammonium-tetrakis(pentafluorophenyl)borate in DCE and 5 mM of LiTB in water). The Galvani potential difference across the interface is fixed at positive potentials. The Galvani potential was calculated and found to be 0.54 V. To perform the two-phase reaction, the reaction flasks were stirred for a certain period. About 20 min after the addition of aqueous solution to the flask containing Fc and compound **1**, the color of solution became green and a new absorption sharp band (at 620 nm) appeared in the UV–Vis spectrum (Figure 6a). However, when only Fc was present in the organic phase, the color of solution

did not change and the increase of Fc^+ absorption bands at 620 nm was marginal (see Figure 6a).

To examine the aqueous phase, an excess amount of KI (equivalent to 0.20 M) was added to the aqueous phase and UV-Vis spectra were measured, which are presented in Figure 6b. The absorption characteristic of triiodide (I_3^-) was observed as an intense band at $\lambda_{\text{max}} = 350$ nm, which confirms the production of hydrogen peroxide (H_2O_2) in the two-phase reaction. When only compound

1 was dissolved in DCE, I_3^- was detected, which is a strong indicator for the production of H_2O_2 in the presence of compound **1**. When both Fc and compound **1** were present, no clear evidence of H_2O_2 was detected (see Figure 6b). In this case, H_2O_2 (0.04 mM) was detected in water, which corresponds to a yield of 5% by considering a two-electron reduction of O_2 (the theoretical yield of H_2O_2 amounts to 0.80 mM). For this reason, the effect of hydrogen peroxide decomposition on the

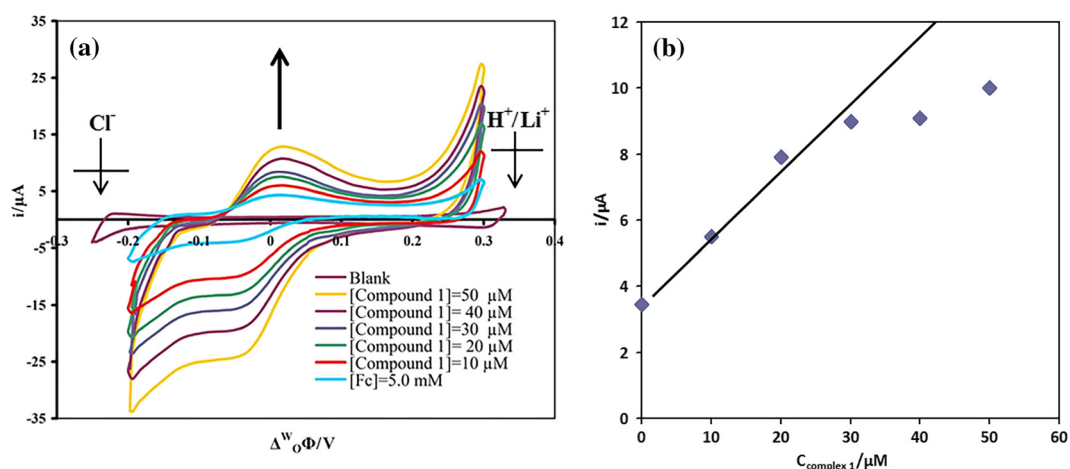
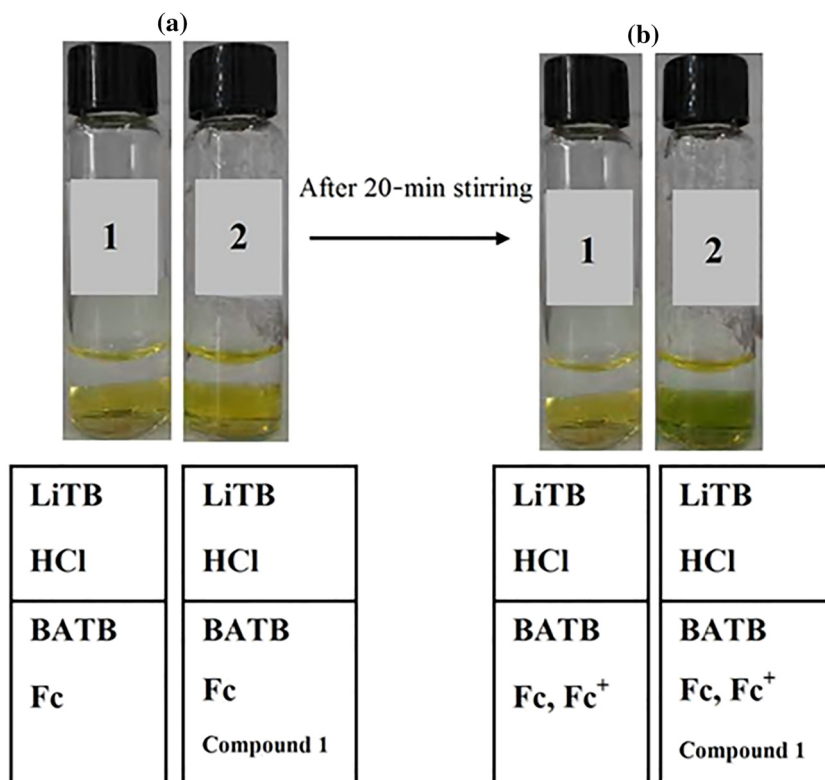


FIGURE 5 (a) Cyclic voltammetry at the water–1,2-dichloroethane (DCE) interface obtained with cell 2 that is illustrated in Scheme 1 in the presence of 5 mM ferrocene (Fc; $y = 5$) and at various concentrations of compound **1**. (b) Linear dependence of the irreversible current at 0.27 V versus compound **1** concentration



SCHEME 3 Photographic illustration of the two-phase reaction. The flasks contained 1) ferrocene (Fc; 4 mM) and 2) compound **1** (50 μM) and ferrocene (Fc; 4 mM) in the 1,2-dichloroethane (DCE) solutions. The aqueous solution of both flasks contained LiTB (5 mM) and HCl (10 mM)

observed selectivity for two-electron reduction of O_2 was studied. The following experiment was carried out in the mixture of equal volumes of DCE solution containing Fc and compound **1** as well as aqueous hydrogen peroxide solution (Scheme 4). The amount of hydrogen peroxide was determined with the KI method, which indicated that the amount of hydrogen peroxide decreased to 50% after 20 min. This result indicates that the reduction of O_2 is a direct four-electron reduction to H_2O ^[27] catalyzed by a mixture of compound **1** and Fc and the formation of H_2O_2 via a two-electron reduction pathway in the presence of compound **1**.

3.6 | Kinetic information

Figure 7 shows the time profile of the absorbance in the absence and presence of the catalyst at 620 nm. Kinetic

data obtained from the experiments for Fc and Fc + compound **1** are shown in Figure 7a. Assuming the first-order reaction, the reaction rate can be written as follows:

$$v = k[Fc] \quad (1)$$

where k is the rate constant of the reaction. The integrated rate law is expressed as

$$kt = \ln \frac{[Fc]}{([Fc] - [Fc]^+)} \quad (2)$$

As shown in Figure 7b, the slopes of the straight lines represent the rate constants (k/s). It can be clearly seen that the rate of the reaction increases in the presence of

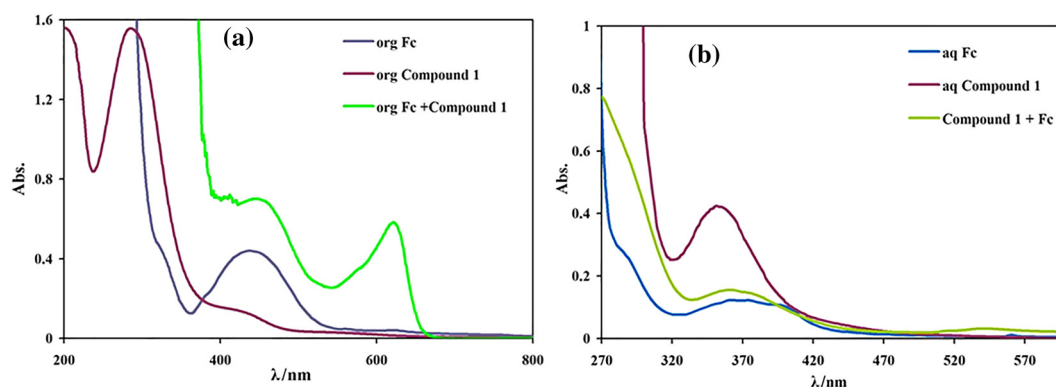
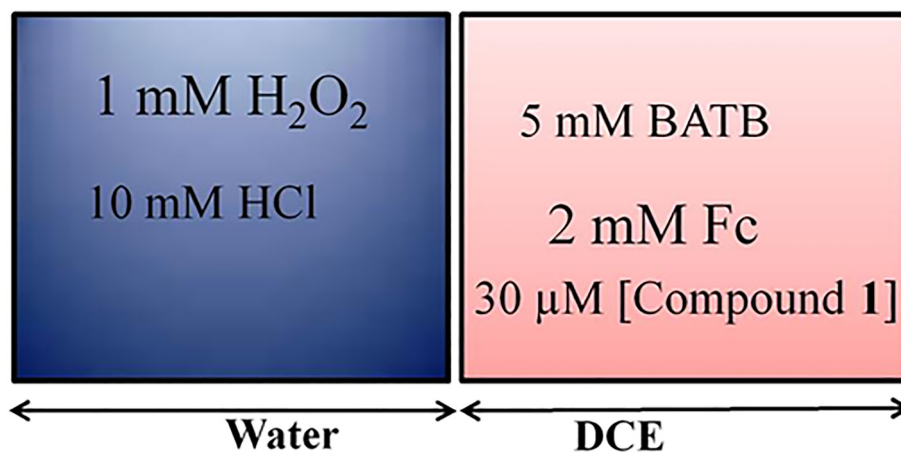


FIGURE 6 (a) UV-Vis spectra of compound **1** in 1,2-dichloroethane (DCE; red line) and after separation from the aqueous phase, where the top aqueous phase contains 5 mM of LiTB and 10 mM of HCl, and the bottom DCE phase contains 5 mM of bis(triphenylphosphoranylidine)ammonium-tetrakis(pentafluorophenyl)borate (BATB) and 50 μ M of compound **1**; UV-Vis spectra of DCE solutions containing 4 mM of ferrocene (Fc; blue line) after two-phase reaction and separation from each other, 4 mM of Fc along with 50 μ M of compound **1** (green line); (b) UV-Vis spectra of the aqueous solutions after being treated with an excess amount of potassium iodide, compound **1** (50 μ M) (red line), Fc (4 mM) (blue line), and Fc (4 mM) + compound **1** (50 μ M) (green line)



SCHEME 4 The initial composition of the aqueous phase and the organic phase for studying hydrogen peroxide decomposition in a biphasic reaction. DCE, 1,2-dichloroethane; Fc, ferrocene

compound **1**. The oxidation of Fc is faster in the presence of compound **1**; consequently, the O₂ reduction rate is increased.

The rate of the reaction in the presence of compound **1** was increased 24.87 times (Table 4). A comparison between the catalytic effect of compound **1** and the previously reported CoL^[11] shows that compound **1** is a

stronger catalyst than CoL. CoL has one cobalt core, whereas compound **1** has two cores. The use of multinuclear compounds can facilitate multielectron transfer and increase the rate constant of reaction.^[43]

Because compound **1** has nitrogen containing groups in its structure, this compound may also have a proton transfer role at the liquid–liquid interface. Proton affinity

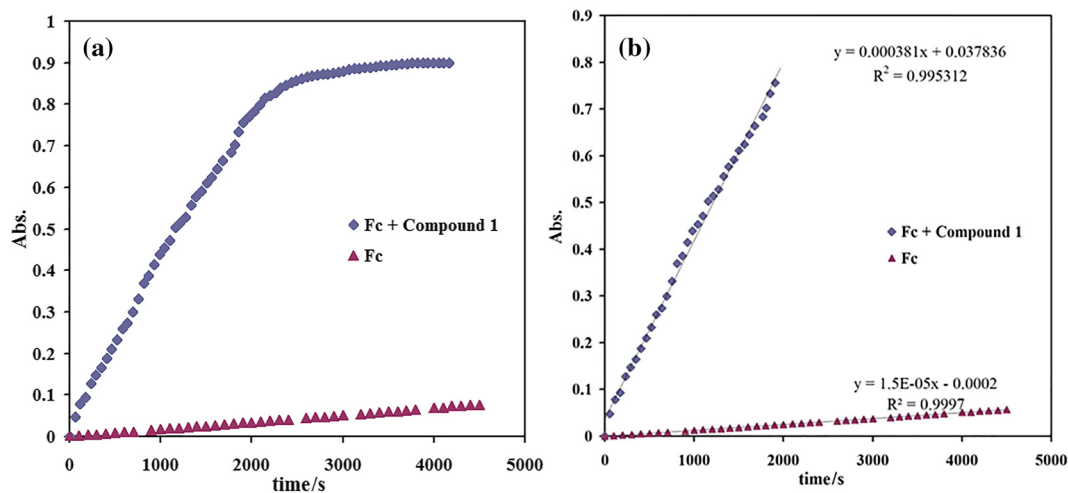
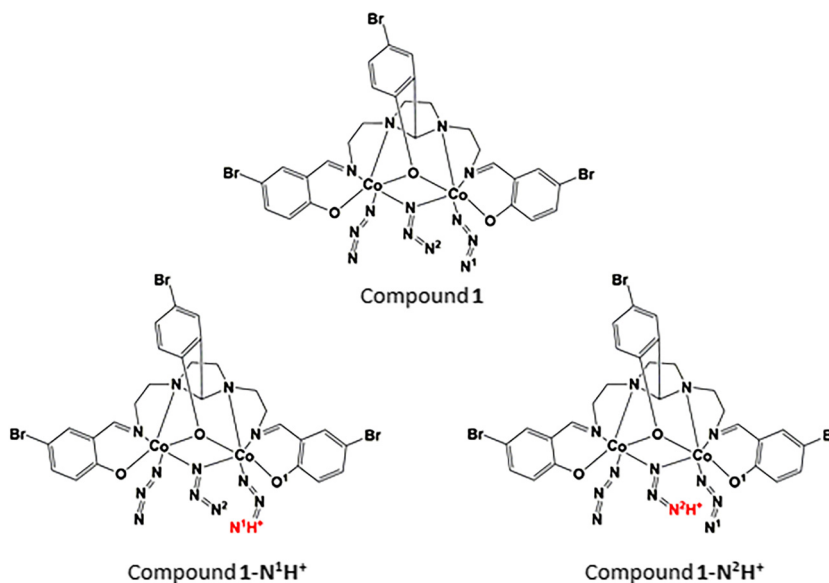


FIGURE 7 (a) Kinetics of the biphasic oxidation of ferrocene (Fc; 4 mM) (triangles) and Fc + compound **1** (50 μM) (diamonds) at pH 2 and (b) plot of $\ln\{[Fc]/([Fc]-[Fc^+])\}$ versus time for only Fc (triangles) and Fc + compound **1** (50 μM) (diamonds)

TABLE 4 Comparison between catalytic effect of compound **1** and CoL

Catalyst	Electron donor	pH	Rate constant, k/s^{-1}	Time for shake flask experiment/min	% of conversion	k/k of catalysis	Ref.
CoL ^a	Fc	2	2.03×10^{-4}	50	40	13.53	[11]
Compound 1	Fc	2	3.81×10^{-4}	20	40	25.4	This work

^aOxidative resistant complex of cobalt–hydrazone (CoL)



SCHEME 5 Illustration of various protonated positions of compound **1**

TABLE 5 Proton affinity and gas basicity (GB) of compound **1** at gas state and room temperature calculated by DFT/B3LYP/LANL2DZ level of theory

GB/kJ mol ⁻¹	PA/kJ mol ⁻¹	Species
-2.7289	62.0248	1-N¹H⁺
50.9373	115.8213	1-N²H⁺

DFT, density functional theory.

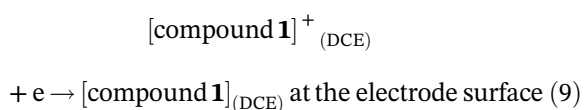
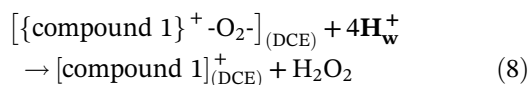
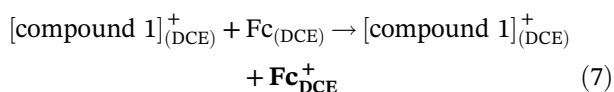
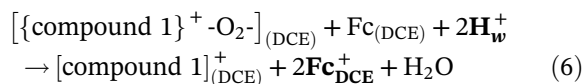
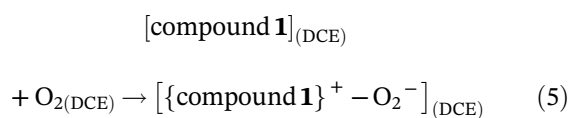
(PA) and gas basicity (GB) are terms that indicate basicity property of one group at the gaseous state. These terms are expressed by equations (3) and (4). The structures of protonated position of compound **1** are indicated in Scheme 5.

$$PA = \Delta H^0_{\text{reactant}} - \Delta H^0_{\text{product}} \quad (3)$$

$$GB = \Delta G^0_{\text{reactant}} - \Delta G^0_{\text{product}} \quad (4)$$

The group with more basic property allows stronger proton transfer to the organic phase. Data in Table 5, obtained by DFT calculations, show that **1-N²** is the best group to facilitate proton transfer to the organic phase. Therefore, **1-N²** has more basic property than **1-N¹**.

The three-step reaction mechanism is proposed based on the aforementioned data. This PCET reaction is preceded and followed by coordination of O₂ to compound **1** and the regeneration of compound **1** by Fc. These steps may be expressed by equations (5)–(7). In the absence of FC, hydrogen peroxide is the main product [equations (8) and (9)].



4 | CONCLUSIONS

In summary, a new dinuclear Co(III) coordination compound was synthesized and characterized by spectroscopic methods and single-crystal X-ray analysis. Because the liquid–liquid interface can be considered a model for biomimetic biomembranes, the catalytic effects of the obtained dinuclear Co(III) coordination compound on the proton-coupled O₂ reduction involving Fc was studied at a water–DCE interface. It was found that compound **1** can catalyze O₂ reduction to H₂O₂, whereas in the presence of Fc, it can catalyze the reduction of O₂ to water. The catalytic kinetic study showed that compound **1** with two cobalt cores is a stronger catalyst than the previously reported mononuclear cobalt coordination compound.

ACKNOWLEDGMENTS

The authors are grateful to the University of Zanjan and Imam Khomeini International University for financial support of this study.

ORCID

Mohammad Ali Kamyabi  <https://orcid.org/0000-0003-4494-3011>

Rahman Bikas  <https://orcid.org/0000-0003-0078-7571>

Nader Noshiranzadeh  <https://orcid.org/0000-0002-8611-8338>

Marzieh Emami  <https://orcid.org/0000-0002-3339-681X>

Tadeusz Lis  <https://orcid.org/0000-0003-0157-0649>

REFERENCES

- [1] R. Boulatov, Billion-year-old oxygen cathode that actually works: Respiratory oxygen reduction and its biomimetic analogs, in *N4-Macrocyclic Metal Complexes*, Springer, New York, **2006** 1.
- [2] S. Rastgar, H. Deng, F. Cortés-Salazar, M. D. Scanlon, M. Pribil, V. Amstutz, A. A. Karyakin, S. Shahrokhian, H. H. Girault, *Chem. Electro. Chem.* **2014**, *1*, 59.
- [3] D. Xiang, X. Bo, X. Gao, C. Du, P. Li, L. Zhu, W. Chen, *J. Colloid Interface Sci.* **2019**, *534*, 655.
- [4] M. Liu, C. Cai, J. Li, J. Zhao, W. Teng, R. Liu, *J. Colloid Interface Sci.* **2018**, *528*, 1.
- [5] B. Su, I. Hatay, A. N. Trojánec, Z. Samec, T. Khoury, C. P. Gros, J.-M. Barbe, A. Daina, P.-A. Carrupt, H. H. Girault, *J. Am. Chem. Soc.* **2010**, *132*, 2655.
- [6] X. Shi, J. Song, F. Zhao, H. Gao, X. Chen, P. Chen, Z. An, Y. Chen, *J. Colloid Interface Sci.* **2019**, *533*, 569.
- [7] S. Fukuzumi, K. Okamoto, Y. Tokuda, C. P. Gros, R. Guilard, *J. Am. Chem. Soc.* **2004**, *126*, 17059.

- [8] T. Honda, T. Kojima, S. Fukuzumi, *J. Am. Chem. Soc.* **2012**, *134*, 4196.
- [9] H. H. Girault, Charge Transfer across Liquid—Liquid Interfaces, in *Modern Aspects of Electrochemistry*, (Eds: J. O. M. Bockris, B. E. Conway, R. White), Springer, US **1993** 1.
- [10] W. Adamiak, J. Jedraszko, O. Krysiak, W. Nogala, J. C. Hidalgo-Acosta, H. H. Girault, M. Opallo, *J. Phys. Chem.* **2014**, *118*, 23154.
- [11] M. A. Kamyabi, F. Soleymani-Bonoti, R. Bikas, H. Hosseini-Monfared, N. Arshadi, M. Siczek, T. Lis, *Phys. Chem. Chem. Phys.* **2015**, *17*, 32161.
- [12] V. J. Cunnane, G. Geblewicz, D. J. Schiffrin, *Electrochim. Acta* **1995**, *40*, 3005.
- [13] M. A. Kamyabi, F. Soleymani-Bonoti, R. Bikas, H. Hosseini-Monfared, *J. Electroanal. Chem.* **2017**, *794*, 235.
- [14] F. Soleymani-Bonoti, M. A. Kamyabi, N. Arshadi, *Comput. Theor. Chem.* **2016**, *1092*, 47.
- [15] X. Liu, S. Wu, B. Su, *J. Electroanal. Chem.* **2013**, *709*, 26.
- [16] Y. Xuan, X. Huang, B. Su, *J. Phys. Chem.* **2015**, *119*, 11685.
- [17] H. Ohde, K. Maeda, Y. Yoshida, S. Kihara, *J. Electroanal. Chem.* **2000**, *483*, 108.
- [18] D. Saha, T. Maity, R. Bera, S. Koner, *Polyhedron* **2013**, *56*, 230.
- [19] S. Bhunia, S. Jana, D. Saha, B. Dutta, S. Koner, *Catal. Sci. Technol.* **2014**, *4*, 1820.
- [20] A. M. Ullman, C. N. Brodsky, N. Li, S.-L. Zheng, D. G. Nocera, *J. Am. Chem. Soc.* **2016**, *138*, 4229.
- [21] S. Lin, C. S. Diercks, Y.-B. Zhang, N. Kornienko, E. M. Nichols, Y. Zhao, A. R. Paris, D. Kim, P. Yang, O. M. Yaghi, *Science* **2015**, *349*, 1208.
- [22] T. J. Korstanje, J. I. van der Vlugt, C. J. Elsevier, B. de Bruin, *Science* **2015**, *350*, 298.
- [23] J. Schneidewind, R. Adam, W. Baumann, R. Jackstell, M. Beller, *Angew. Chem. Int. Ed.* **2017**, *56*, 1890.
- [24] A. Mukherjee, D. Srimani, S. Chakraborty, Y. Ben-David, D. Milstein, *J. Am. Chem. Soc.* **2015**, *137*, 8888.
- [25] J.-M. Lei, S.-P. Luo, S.-Z. Zhan, *Polyhedron* **2018**, *154*, 295.
- [26] J.-W. Wang, K. Yamauchi, H.-H. Huang, J.-K. Sun, Z.-M. Luo, D.-C. Zhong, T.-B. Lu, K. Sakai, *Angew. Chem. Int. Ed.* **2019**, *58*, 10923.
- [27] I. Hatay, B. Su, F. Li, M. A. Méndez, T. Khoury, C. P. Gros, J.-M. Barbe, M. Ersoz, Z. Samec, H. H. Girault, *J. Am. Chem. Soc.* **2009**, *131*, 13453.
- [28] P. Peljo, L. Murtomäki, T. Kallio, H.-J. Xu, M. Meyer, C. P. Gros, J.-M. Barbe, H. H. Girault, K. Laasonen, K. S. Kontturi, *J. Am. Chem. Soc.* **2012**, *134*, 5974.
- [29] R. Partovi-Nia, B. Su, M. A. Méndez, B. Habermeyer, C. P. Gros, J. M. Barbe, Z. Samec, H. H. Girault, *Chem. Phys. Chem.* **2010**, *11*, 2979.
- [30] R. Partovi-Nia, B. Su, F. Li, C. P. Gros, J. M. Barbe, Z. Samec, H. H. Girault, *Chem. – Eur. J.* **2009**, *15*, 2335.
- [31] S. Fukuzumi, S. Mandal, K. Mase, K. Ohkubo, H. Park, J. Benet-Buchholz, W. Nam, A. Llobet, *J. Am. Chem. Soc.* **2012**, *134*, 9906.
- [32] I. H. Patir, *Electrochim. Acta* **2013**, *87*, 788.
- [33] A. Trojánek, V. Mareček, H. Jänchenová, Z. Samec, *Electrochem. Commun.* **2007**, *9*, 2185.
- [34] V. J. Cunnane, D. J. Schiffrin, C. Beltran, G. Geblewicz, T. Solomon, *J. Electroanal. Chem. Interfacial Electrochem.* **1988**, *247*, 203.
- [35] R. Bikas, E. Shahmoradi, N. Noshiranzadeh, M. Emami, S. Reinoso, *Inorg. Chim. Acta* **2017**, *466*, 100.
- [36] N. Noshiranzadeh, M. Emami, R. Bikas, A. Kozakiewicz, *New J. Chem.* **2017**, *41*, 2658.
- [37] N. Noshiranzadeh, R. Bikas, K. Ślepokura, M. Shaabani, T. Lis, *J. Fluorine Chem.* **2014**, *160*, 34.
- [38] R. Bikas, H. H. Monfared, T. Lis, M. Siczek, *Inorg. Chem. Commun.* **2012**, *15*, 151.
- [39] N. Noshiranzadeh, R. Bikas, K. Ślepokura, M. Mayeli, T. Lis, *Inorg. Chim. Acta* **2014**, *421*, 176.
- [40] R. Bikas, F. Ajormal, M. Emami, J. Sanchiz, N. Noshiranzadeh, A. Kozakiewicz, *Polyhedron* **2019**, *162*, 20.
- [41] M. Emami, R. Bikas, N. Noshiranzadeh, J. Sanchiz, K. Ślepokura, T. Lis, *J. Mol. Struct.* **2019**, *1180*, 392.
- [42] Y. K. Choi, J. K. Park, S. Jeon, *Electroanal. Int. J. Devoted Fundam. Pract. Aspects Electroanal.* **1999**, *11*, 134.
- [43] J. P. Collman, P. Denisevich, Y. Konai, M. Marrocco, C. Koval, F. C. Anson, *J. Am. Chem. Soc.* **1980**, *102*, 6027.

SUPPORTING INFORMATION

Additional supporting information may be found online in the Supporting Information section at the end of this article.

How to cite this article: Kamyabi MA, Soleymani-Bonoti F, Alirezaei F, et al. Electrocatalytic properties of a dinuclear cobalt(III) coordination compound in molecular oxygen reduction reaction. *Appl Organometal Chem.* 2019; e5214. <https://doi.org/10.1002/aoc.5214>

APPENDIX A

CCDC 1864764 contains the supplementary crystallographic data for compound **1**. These data can be obtained free of charge from The Cambridge Crystallographic Data Centre via www.ccdc.cam.ac.uk/data_request/cif. Electronic supporting information file of this article is available online at: